FORSCHUNGSZENTRUM
ROSSENDORF e.V.

FZR

FZR-121
Januar 1996

H. Kumpf and K. Noack

Application of the Guiding Centre Approximation to the Transport of Injected Fast Ions in a Mirror Based Plasma Neutron Source

Forschungszentrum Rossendorf e.V.
Postfach 51 01 19 · D-01314 Dresden
Bundesrepublik Deutschland

Telefon (0351) 260 3467
Telefax (0351) 260 3440
E-Mail kumpf@fz-rossendorf.de

Application of the Guiding Centre Approximation to the Transport of Injected Fast Ions in a Mirror Based Plasma Neutron Source

H. Kumpf, K. Noack

Forschungszentrum Rossendorf e.V.

Abstract

The guiding centre approximation for the motion of charged particles in axially symmetric magnetic and electric fields is formulated and stopping as well as small angle scattering on a multicomponent plasma are included. The developed code has been applied to the design of a 14-MeV neutron source according to the concept of the Budker Institute Novosibirsk. It is demonstrated that the self-interaction of injected D and T ions by stopping, scattering and induced internal fields has to be taken into account, if the injected power exceeds a few megawatt.

Contents

1 Introduction

The present paper can be viewed as a part of the efforts made commonly by the Budker Institute Novosibirsk and FZR for demonstrating the feasibility of an intense 14-MeV neutron source based on the Novosibirsk concept of an open trap. Recently the whole subject has been presented in a broader context in [1].

The special topic here is the modelling of the transport of the fast ions originating from the injected neutral atoms of the hydrogen isotopes by ionization in the target plasma. The method adopted here is the well known guiding centre approximation (g.c.a.), adapted to cylinder coordinates and axially symmetric fields. Of course, one could instead integrate numerically the particles equations of motion with the Lorentz force as the right hand side, although in this case one has to take special care in order to conserve the necessary accuracy even after some 10^5 Larmor revolutions performed by the ion during its life. But the g.c.a. seems to offer advantages in terms of computing time. At the same time the accuracy of the g.c.a. approach adopted here is amply sufficient, as has been demonstrated by comparison with results from the direct integration.

The interaction of the fast ions with the plasma is taken into account by means of the relaxation times τ_b and τ_d for stopping and deflection in a multicomponent plasma including the population of the fast ions themselves.

The only place where random numbers are used is in the description of small angle scattering. But for as long as Coulomb scattering does not play a decisive role, the statistical error in the final results due to this randomness is insignificant ($< 5\%$ in the example considered).

2 Recapitulation of the guiding centre approximation

There exist several formulations of guiding centre approximations in the literature, some of them differing in certain details. We adopt the version of ref.[2]. In the following we recall briefly the essence of the method, in order to introduce the terminology. The meaning of symbols is repeated in the index of notations at the end of the paper.

The method starts with a series of transformations of the dynamic variables of the particle:

$$(\vec{q},\vec{v}) \Rightarrow (\vec{q},v_\parallel,v_\perp,\varphi) \Rightarrow (\vec{q},\mathcal{E},\mu,\varphi) \Rightarrow (\vec{Y},\mathcal{E},M,\Phi)$$

In the first of the above transformations the particle velocity $\vec{v}$ is represented by its components parallel ($v_\parallel$) and perpendicular ($v_\perp$) to a given external magnetic field $\vec{B} = B\vec{b}$, as well as by its phase φ, the angle between the perpendicular component and the binormal to the field line at point $\vec{q}$. The quantity μ after the second transformation, called the magnetic moment of the Larmor rotation is defined by

$$\mu = \frac{mv_\perp^2}{2B(\vec{q})} \tag{1}$$

In the last step, the transformation to guiding centre coordinates $(\vec{Y},\mathcal{E},M,\Phi)$ a small parameter ϵ is included artificially by making the following replacement in the equations of motion:

$$\Omega = \frac{eB}{mc} \quad \longrightarrow \quad \frac{\Omega}{\epsilon} \tag{2}$$

All quantities are expanded up to first order in ϵ; afterwards is set $\epsilon = 1$. The physical picture behind this procedure is the assumption, that the time scale of an "average" motion is large compared to the time scale of the Larmor rotation $1/\Omega$.
The natural guiding centre variables $(\vec{Y},\mathcal{E},M,\Phi)$ are defined by:

$$\vec{Y} = \vec{q} + \epsilon\vec{\rho}_1(\vec{q},\mathcal{E},\mu,\varphi) + O(\epsilon^2) \tag{3}$$

$$M = \mu + \epsilon\mu_1(\vec{q},e,\mu,\varphi) + O(\epsilon^2) \tag{4}$$

$$\Phi = \varphi + \epsilon f_1(\vec{q},\mathcal{E},\mu,\varphi) + O(\epsilon^2) \tag{5}$$

and the unknown functions $\vec{\rho}_1, \mu_1, f_1$ are determined by the *condition that the right hand sides of the equations of motion for the guiding centre variables be independent of* Φ.
$\vec{q}, \mathcal{E}, \mu, \varphi$ or $\vec{q}, v_\parallel, v_\perp, \varphi$ are called particle variables.
$\vec{Y}, \mathcal{E}, M, \Phi$ are called (natural) guiding centre variables.
Unfortunately, the specialization of the general formulation of the guiding centre approximation contained in [2] to cylinder coordinates $\vec{Y} = (Y_\rho, Y_\psi, Y_z)$, $\vec{q} = (\rho, \psi, z)$ leads to essential singularities at $\rho = 0$. One arrives at a valid formulation by replacing condition (5) with:

$$\Phi = \varphi - \psi + \epsilon f_1(\vec{q}, \mathcal{E}, \mu, \varphi) + O(\epsilon^2) \tag{6}$$

and repeating the derivations from [2] for the special case of cylinder coordinates. The result is stated in the next two subsections.

2.1 Transformation equations $\vec{Y}, \mathcal{E}, M, \Phi \longrightarrow \vec{q}, v_\perp, v_\parallel, \varphi$

$$Y_z = z + \frac{v_\perp b_\rho \cos\varphi}{\Omega} \tag{7}$$

$$Y_\rho \cos(Y_\psi - \psi) = \rho - \frac{v_\perp b_z \cos\varphi}{\Omega} \tag{8}$$

$$Y_\rho \sin(Y_\psi - \psi) = \frac{v_\perp \sin\varphi}{\Omega} \tag{9}$$

$$\mathcal{E} = \frac{m}{2}(v_\perp^2 + v_\parallel^2) + e\phi \tag{10}$$

$$M = \frac{m v_\perp^2}{2B} - \frac{m}{\Omega B}\left[-v_\perp(v_\parallel^2 + v_\perp^2/2)\cos\varphi\, B_- - \frac{1}{2} v_\parallel v_\perp^2 \sin\varphi\cos\varphi\, B_+\right] + \frac{e}{m} v_\perp \cos\varphi\, E_- \tag{11}$$

$$\Phi = \varphi - \psi + \frac{1}{\Omega}\left[-\frac{v_\perp^2 + v_\parallel^2}{v_\perp}\sin\varphi\, B_- + \frac{v_\perp(b_z - 1)\sin\varphi}{\rho} + \frac{e\sin\varphi}{m v_\perp} E_- + \frac{1}{4} v_\parallel(\cos^2\varphi - \sin^2\varphi) B_+\right] \tag{12}$$

The field quantities $B, b_z, b_\rho, \Omega, \phi, E_\rho, E_z$ depend on the particle coordinates (ρ, z) . Here B, b_z, b_ρ represent the intensity and the components of the direction of the magnetic field, E_ρ, E_z the components of the electric field, ϕ the electric potential. The following abbreviations for expressions containing the derivatives of the fields have been used:

$$\begin{aligned} B_- &= \left(b_z \frac{\partial B}{\partial \rho} - b_\rho \frac{\partial B}{\partial z}\right)/B \\ E_- &= b_z E_\rho - b_\rho E_z \\ B_+ &= \left(b_z \frac{\partial B}{\partial z} + b_\rho \frac{\partial B}{\partial \rho}\right)/B + 2b_\rho/\rho \end{aligned} \tag{13}$$

2.2 Equations of motion for guiding centre coordinates

$$\dot{Y}_\rho = U b_\rho \tag{14}$$

$$\dot{Y}_\psi = \frac{1}{Y_\rho \Omega}(U^2 B_- + M B B_-/m - e E_-/m) \tag{15}$$

$$\dot{Y}_z = U b_z \tag{16}$$

$$\dot{\Phi} = \Omega \tag{17}$$

$$\dot{\mathcal{E}} = 0 \tag{18}$$

$$\dot{M} = 0 \tag{19}$$

$$\text{with} \qquad U = \pm\sqrt{\frac{2}{m}(\mathcal{E} - e\phi - MB)} \tag{20}$$

In contrast to the preceding set of the transformation equations in these equations of motion the field quantities $B, b_z, b_\rho, \Omega, \phi$ as well as the derived expressions B_-, E_- defined above are to be understood as functions of the guiding centre coordinates Y_ρ, Y_ψ, Y_z.

At first glance one might suppose a singularity at $Y_\rho \to 0$. But due to axial symmetry and the Maxwell equations all of $b_\rho, \partial B/\partial\rho, E_\rho \to 0$ as $Y_\rho \to 0$.

Inspecting the above equations (14-20) one sees immediately that there is no dependence on Φ. Their form is extremely simplified and their number reduced. As a consequence integration may be done in large steps and no numerical troubles are to be expected. All these pleasant features are in contrast to the case of directly using the equations of motion for the particle coordinates. The fast Larmor rotation (dependence on φ) is now contained in the transformation equations of the preceding paragraph alone. But those are nondifferential equations, which can be solved by a few iteration steps.

Comment: The guiding centre approximation comprises a number of phenomena: centrifugal drift, grad$B$ drift and *nonconservation of the magnetic moment* μ.

3 Slowing down and small angle scattering in the framework of the guiding centre approximation

Energy $\mathcal{E}$ and mean square deflection angle $\langle\vartheta^2\rangle$ obey

$$\frac{d\mathcal{E}}{dt} = -\frac{\mathcal{E}}{\tau_b} \tag{21}$$

$$\frac{d\langle\vartheta^2\rangle}{dt} = \frac{1}{\tau_d} \tag{22}$$

The dependence of the relaxation times τ_b and τ_d on local plasma parameters like electron and ion temperatures, density and plasma composition is stated by Trubnikov [3] and others. The problem is how slowing down and scattering influence the guiding centre coordinates. Let us first evaluate the changes of the particle coordinates due to stopping and deflection and afterwards translate them into changes of the guiding centre coordinates by means of the transformation expressions in zero order.

3.1 Change of generalized magnetic moment M due to scattering

The laws of binary scattering for deflection by a polar angle ϑ and azimuthal angle γ lead to the following expression for the relative change Δ of the generalized moment M:

$$\Delta = \frac{M' - M}{M} = A\vartheta^2 - \xi^2\vartheta^2 - 2\sqrt{A}\xi\vartheta\left(1 - \frac{\vartheta^2}{2}\right) \tag{23}$$

$$\text{where} \quad \xi = \cos\gamma \tag{24}$$

$$\text{and} \quad A = \frac{\mathcal{E}}{MB} - 1 = \frac{v_\parallel^2}{v_\perp^2}. \tag{25}$$

Now, ϑ is distributed according to:

$$f_\vartheta(\vartheta) = \frac{2\vartheta}{\langle\vartheta^2\rangle} \exp\left(-\frac{\vartheta^2}{\langle\vartheta^2\rangle}\right) \qquad \text{for} \qquad 0 \leq \vartheta < \infty, \tag{26}$$

where $\langle\vartheta^2\rangle$ is evaluated in eq.(22).

On the other hand, γ is distributed uniformly in $0 \leq \gamma \leq 2\pi$, for which reason:

$$f_\xi(\xi) = \frac{1}{\pi\sqrt{1-\xi^2}} \qquad \text{for} \qquad -1 \leq \xi \leq 1. \tag{27}$$

Therefore the distribution for the relative change Δ of the constant of motion M due to scattering reads:

$$f_\Delta(\Delta) = \frac{2}{\pi\langle\vartheta^2\rangle} \int \delta\left(\Delta - A\vartheta^2 + \xi^2\vartheta^2 + 2\sqrt{A}\xi\vartheta\left(1 - \frac{\vartheta^2}{2}\right)\right) \frac{\vartheta e^{-\vartheta^2/\langle\vartheta^2\rangle}}{\sqrt{1-\xi^2}}\, d\vartheta\, d\xi, \tag{28}$$

where $\delta(x)$ stands for the Dirac deltafunction. There is no obvious way to make the distribution explicit. However, its mean $\bar{\Delta}$ and mean square deviation σ^2 are easily evaluated:

$$\bar{\Delta} = \int \Delta f_\Delta(\Delta)\, d\Delta = \left(A - \frac{1}{2}\right)\langle\vartheta^2\rangle \tag{29}$$

$$\sigma^2 = \int (\Delta - \bar{\Delta})^2 f_\Delta(\Delta)\, d\Delta = 2A\langle\vartheta^2\rangle + \left(2A^3 - A^2 - 5A + \frac{1}{2}\right)\langle\vartheta^2\rangle^2 \tag{30}$$

A more detailed investigation shows, that for $A \gg \langle\vartheta^2\rangle$, i.e. a bit away from the turning points of the orbit, the distribution for Δ has the form of a Gaussian with the parameters cited above. At the turning points themselves this distribution is an exponential one for the interval $-\infty < \Delta < 0$. But as the regions around the end points hardly contribute to the overall smearing out of the orbit, for practical purposes one may generally adopt the Gaussian form with proper mean and dispersion.

The above equations demonstrate $\bar{\Delta}$ and σ to be of the same order. Therefore a deterministic treatment of small angle scattering is insufficient, and one has to resort to a Monte Carlo simulation.

In concluding the treatment of the change of the magnetic moment M due to Coulomb scattering we check the sign of $\bar{\Delta}$ from eq.(29) with the help of the definition (25). It shows up that:

$$\bar{\Delta} > 0 \text{ if } v_\parallel^2 > v_\perp^2/2 \qquad \text{and} \qquad \bar{\Delta} < 0 \text{ if } v_\parallel^2 < v_\perp^2/2$$

Thus scattering tends to establish equipartition of energy between one degree of freedom for the motion parallel to the field and two degrees of freedom for perpendicular motion. After all it is comforting to see a general principle confirmed!

3.2 Change of guiding centre coordinates due to stopping

Stopping and scattering induce via changes in the velocity components $v_\perp$ and $v_\parallel$ a shift in the guiding centre space coordinates Y_ρ and Y_z (diffusion in a magnetic field). As the stopping time τ_b is much shorter than the deflection time τ_d for energies considered here ($\mathcal{E} > 3keV$), stopping determines the process. Including scattering at this point would make sense only in the case if straggling, i.e. fluctuations in the stopping process were considered too.

Now, as the direction of $\vec{v}$ is not changed by mere stopping ,

$$\frac{d\mathcal{E}}{dt} = -\frac{\mathcal{E}}{\tau_b} \text{ leads to } \frac{dv_\perp}{dt} = -\frac{v_\perp}{2\tau_b}. \tag{31}$$

The combination of eq.(8) with (9) leads to:

$$Y_\rho^2 = \left(\rho - \frac{v_\perp b_z \cos\varphi}{\Omega}\right)^2 + \left(\frac{v_\perp \sin\varphi}{\Omega}\right)^2 \tag{32}$$

This combined with eq.(31) yields up to first order in $1/\Omega$:

$$\frac{dY_\rho^2}{dt} = \frac{v_\perp b_z \rho \cos\varphi}{\tau_b \Omega} \tag{33}$$

Likewise:

$$\frac{dY_z}{dt} = -\frac{v_\perp b_\rho \cos\varphi}{2\tau_b \Omega} \tag{34}$$

4 Code implementation for axially symmetric fields

The principal structure of the implemented code will be explained by means of the block diagram fig.1. The directions of the arrows generally show the corresponding calls. The only exceptions are the arrows connected with the dashed boxes, representing flow of data. The subroutine MOVER simulates the ionization process of the impinging beam of neutral atoms and generates the initial particle as well as guiding centre coordinates using eq.(7-12). The equations of motion (14-20) are then solved by a standard method in steps of several Larmor turns. Due to the smoothness of the guiding centre motion there are no such numerical problems as with direct treatments of the particle's motion.

For calculating the right hand sides of these equations the subroutine FIELDS evaluates the magnetic and electric fields by cubic spline interpolation from numeric tables. These tables on their part have been composed by means of previous calculations based on the distribution of currents in the coils of the plasma device.

Before the next integration step is performed, the subroutine TRAPINT calculates small changes to $\mathcal{E}, M, \vec{Y}$ by means of an integration along the particle orbit according to the expressions derived in section 3. The integration is performed by the trapeze rule with automatic accuracy control. The grid points are obtained by linear interpolation of the guiding centre coordinates and solving the inverse transformation equations (7-12) by iteration.

The subroutine TAU realizes a model for the evaluation of relaxation times τ_b and τ_d based on [3] with components of thermal electrons, thermal hydrogen isotopes and fast deuteron and triton ions. The temperatures of the thermal components are put in, the energy distributions have been determined from trial runs.

5 Steps to self-consistence

If the power of the injected beams of deuterons and tritons approaches the level necessary for an intense source of 14 MeV neutrons, the self-interaction among the population of fast ions cannot be neglected any longer. At present the following three branches of feedback are included in an extra routine PRESS (s. fig.1), the fourth one in the routine CROSSIN. Both routines are run off-line after preceding runs of the MAIN code for deuterons and tritons have stored their results in the RESULTS data file:

1. The coefficients of empirical fits to the space distributions of deuteron and triton densities are conveyed to the PLASMA subroutine, where they influence the stopping and deflection times. The energy distributions of both the fast ion species are supposed to depend on the z coordinate only. They are iterated too. Stopping is increased exclusively by the rise

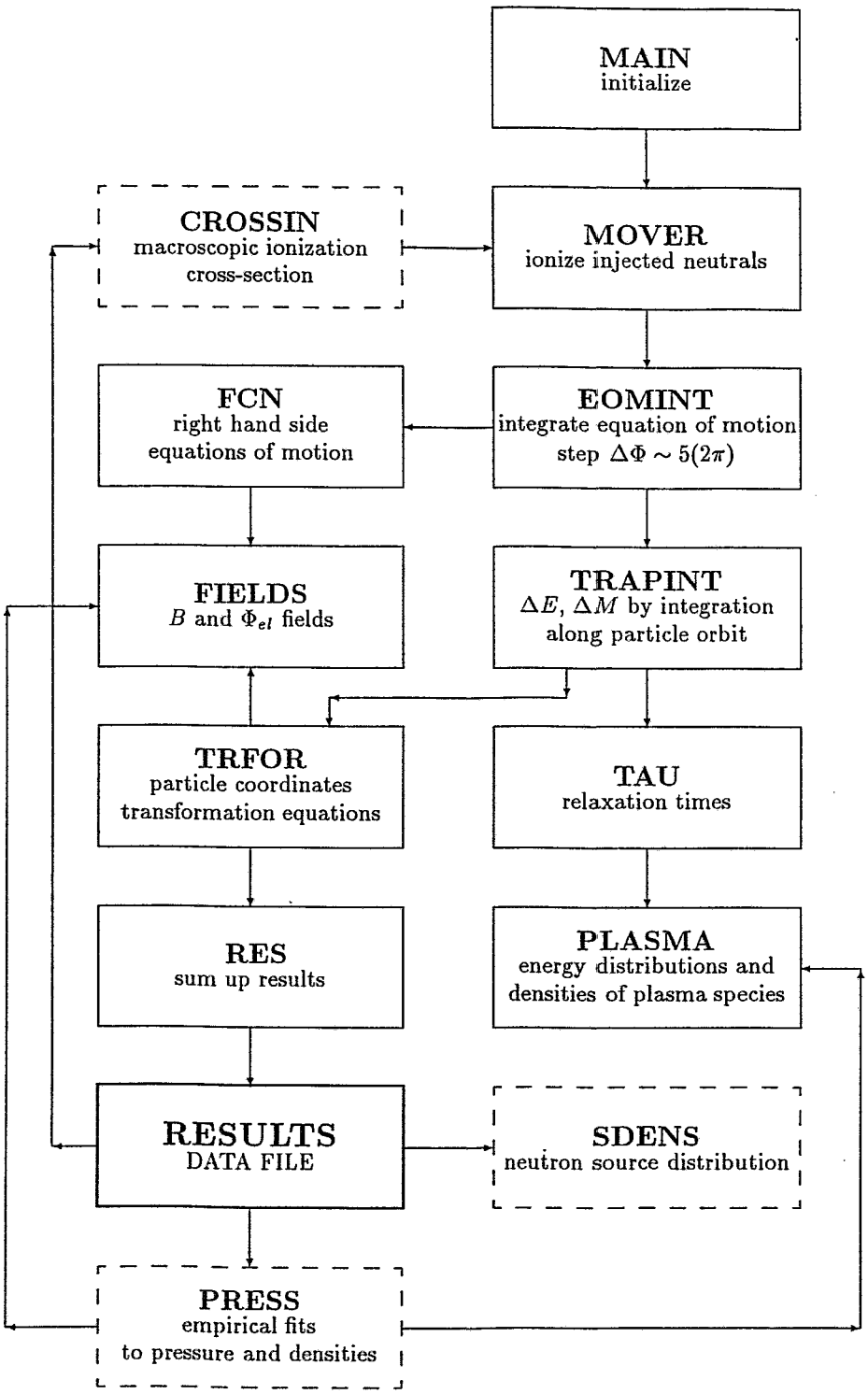

Figure 1: Flow chart of the code

in electron density caused by filling in fast ions. Deflection is influenced by the fast ion populations themselves.

2. The magnetic field $B(r,z)$ inside the plasma is calculated by the following expression, valid in paraxial approximation:

$$B(r,z) = \sqrt{B_{ext}^2(r,z) - 8\pi(p_d + p_t)} \tag{35}$$

Here B_{ext} is the external magnetic field and the pressure p_i of species i $(i = d,t)$ is defined by:

$$p_i(r,z) = \frac{m_i}{2}\overline{n_i(r,z)v_{\perp i}^2(r,z)} \tag{36}$$

The pressures $p_i(r,z)$ are stored in discretized form in the RESULTS data file together with the densities $n_i(r,z)$. In the subroutine FIELDS the r-dependence of the pressure is represented by interpolating expressions.

3. Finally the ambipolar electric potential $\phi(z)$ is evaluated from the condition of electric neutrality:

$$n_{el} = n_{ion} + n_d + n_t, \tag{37}$$

where all the n depend on z only, and n_d as well as n_t are obtained from the RESULTS file by averaging over radius and summing over energy and angle. The electrons as well as the target plasma are supposed to be in thermal equilibrium. Consequently holds:

$$n_{el}(z) = n_{e0}\exp\left[e\phi(z)/T_{el}\right] \qquad \text{and} \qquad n_{ion}(z) = n_{i0}\exp\left[-e\phi(z)/T_{ion}\right] \tag{38}$$

The temperatures T_{el}, T_{ion} as well as the target plasma ion density n_{i0} at the point z_0 where $\phi(z_0) = 0$, e.g. $z_0 = 0$ are supposed to be known. In this respect the code is not totally self-consistent , but should rather be regarded as a part of a future comprehensive code system for the overall design of a mirror neutron source. With known T_{el}, T_{i0}, n_{i0} eq.(37) is a transcendent equation for the unknown ϕ at every point z. The function $\phi(z)$ is then transmitted to the subroutine FIELDS.

4. Last not least the stored densities for deuterons and tritons in the trap are used for calculating the proper distribution of the injection points of D and T ions originating from the impinging beams of neutrals. To this end the following expression for the macroscopic total ionization cross-section Σ_0 is evaluated numerically:

$$\Sigma_0 = \frac{1}{2\pi v_0}\sum_{i=d,t}\int |\vec{v}_0 - \vec{v}_i|\, n_i(E_i,\zeta_i)\left[\sigma_{cx}(E_r) + \sigma_{ion}(E_r)\right] d\,E_i d\,\zeta_i d\,\varphi_i \tag{39}$$

Here the index 0 refers to the impinging atom (D or T), index i to the plasma species d or t. The microscopic cross-sections σ_{cx} and σ_{ion} for charge exchange and ionization respectively are taken from [5]. The further evaluation of the expression for Σ_0 to a certain extent is analogous to the procedure for the d,t-reaction given in the next section.

6 Calculation of neutron source density

The neutron source density N[neutrons/$(m^3 s)$] is expressed as:

$$N = \frac{1}{4\pi^2}\int |\vec{v}_d - \vec{v}_t|\, n_d n_t \sigma_{dt}(E_r)\, dE_d\, dE_t\, d\zeta_d\, d\zeta_t\, d\varphi_d\, d\varphi_t \tag{40}$$

Here E_d, E_t are the deuteron and triton kinetic energies, E_r their relative energy defined below. For both the particle species the following quantities are defined:

$$\zeta = v_{\parallel}/\sqrt{v_{\perp}^2 + v_{\parallel}^2}. \tag{41}$$

and φ_d, φ_t are their phases.

The density n_d has the the following dependences $n_d(E_d, \zeta_d, r, z)$, but is independent of φ_d. The same is true for the index t. Therefore the φ are averaged, whereas the E and ζ are integrated.

Some vector algebraic transformations allow to express the relative velocity $|\vec{v}_d - \vec{v}_t|$ in the variables E, ζ instead of $v_{\parallel}, v_{\perp}$:

$$|\vec{v}_d - \vec{v}_t| = \sqrt{\frac{2E_d}{m_d} + \frac{2E_t}{m_t} - 4\sqrt{\frac{E_d E_t}{m_d m_t}}\left[\zeta_d\zeta_t + \sqrt{(1-\zeta_d^2)(1-\zeta_t^2)}\cos(\varphi_d - \varphi_t)\right]} \tag{42}$$

Once the dependence on φ_d, φ_t is contained exclusively in $\cos\varphi$ with $\varphi = \varphi_d - \varphi_t$ one may transform:

$$\int_0^{2\pi} d\varphi_d \int_0^{2\pi} d\varphi_t \longrightarrow 4\pi \int_0^{\pi} d\varphi$$

The energy of relative motion E_r is defined as

$$E_r = \frac{m_{dt}}{2}(\vec{v}_d - \vec{v}_t)^2, \tag{43}$$

where the reduced mass m_{dt} is defined as

$$m_{dt} = \frac{m_d m_t}{m_d + m_t} \tag{44}$$

and the difference in brackets has already been made explicit in equ.42.

The cross-section of the T(d,n)-reaction $\sigma_{dt}(E_r)$ can be extracted from any neutron data file. Within the energy range concerned here it is also well reproduced by the semiempiric formula [4] :

$$\sigma_{dt}(E_r) = \frac{1.86 \cdot 10^{-68}}{E_r} \frac{\exp(-4,35 \cdot 10^{-7} E_r^{-1/2})}{(E_r - 7.82 \cdot 10^{-15})^2 + 4.38 \cdot 10^{-29}} \tag{45}$$

where E_r and σ_{dt} are measured in SI units. The above formulae are implemented in the code SDENS using the results for the densities n_d and n_t from the main program (s. fig.1). It is operated independently and only after several runs of the main program, when the self-consistent fields have converged.

7 An example

As an example a version has been selected corresponding to a predesign of a plasma neutron source based on the gas dynamic trap proposed by the Efremov Institute St. Peterburg [6]. It has been treated by other methods in the Budker Institute Novosibirsk [8]. Its main characteristic feature is the injection of both reacting species deuterons as well as tritons in the form of atomic beams. The intention here is to keep the injection energy so low as to allow the use of positve ion sources with their much better energy efficiency in comparison to that of negative ion sources [7] .

Here the input for the calculation.

The magnetic field on the axis of the configuration is shown in the fig.2 .

The injection angle amounts to $\theta = 40^0$, for both injected deuterium and tritium beams.

In the right hand part the dependence of the magnetic field in fig.2 exhibits a characteristic threshold in front of the mirror, designed for raising the ion densities and therefore the neutron yield in this region. This is achieved by chosing the ratio of the magnetic field B_{th} at the plateau to its value B_0 at the injection point in the centre according to:

$$\sin(\theta) = \sqrt{\frac{B_0}{B_{th}}} \tag{46}$$

In this case the turning points at least of the freshly injected ions are located in the centre of the hump.

The energies of the beams are $W_d = 80keV$ and $W_t = 94keV$ for deuterium and tritium respectively, the corresponding trapped powers $P_d = 14MW$ and $P_t = 12MW$.

The plasma radius is defined by means of a limiter with $r_0 = 0.085m$ radius, placed at $z = 0$.

The temperatures for ions and electrons of the thermal component of the target plasma are supposed to be $T_i = 6keV$ and $T_e = 1.1keV$ respectively, its density $n_0 = 2.3 \cdot 10^{19} m^{-3}$.

The above example has been treated by the codes represented in the preceding sections. The number of iterations necessary varied from about four for low input power to about seven for higher one. Convergence was considerably accelerated by recalculating the RESULT for deuterons and tritons in turn instead of recalculating both of them at once.

If one tries to solve the original task one obtains erratic behaviour of the result, i.e. no convergence. Only after considerable reduction of the input power level of the d and t neutral beams the dependence of the 14 MeV neutron yield in figure 3 can be calculated. At 5 and 10% of the original power level the obtained dependences still resemble what one might expect from models without feedback. At 20% the neutron yield distribution is unsuitable for a real neutron source.

The apparent solution is to lower the angle of neutral injection (or if this should be linked with unsurmountable technical difficulties to raise the height of the threshold in the magnetic field). The next figure 4 shows the case of 37.5^0 instead of the designed value of 40^0. Here the yield distribution at 20% input power still has the desired shape with a broad peak in the region of the threshold and much less yield outside.

The effect of a further reduction of the injection angle to 35^0 and 32.5^0 repectively demonstrate figures 5 and 6. At 35^0 it is well possible to approach the final power level, although the distributions are still peaked rather sharply. Finally at 32.5^0 injection even the curves for 80 and 100% power input show broad peaks in the vicinity of the threshold and much less yield outside this region. The true optimal angle of injection for $P_d = 14MW$, $P_t = 12MW$ probably is still slightly less than 32.5^0.

Of course there exist ample possibilities for trying to optimize the neutron output. An attempt in this direction demonstrates fig.7, where the input energies of the neutrals have been varied. As might be expected from the energy dependence of the d-t-cross-section no increase of the neutron yield is observed if the input d and t energies are increased. Reducing these energies even leads to smaller output. Thus the accepted values should be close to optimal ones. Of course, a thorough optimization of the neutron yield with respect to injection parameters angle and energy would need a much finer mesh.

The next figures demonstrate some properties of the d and t plasma components in the trap for the near optimal case of 14/12 MW injection power and 32.5^0 injection angle.

Generally it may be stated, that for the most favourable case cited in the last figure the total neutron yield in the region extended 2m around the peak amounts to about 3.8E17 neutrons/s or 0.9 MW, corresponding to an efficiency of energy conversion from neutral beam power to neutron power in the peak of about 3.8%. The shape of the yield distribution along the axis of the device too is rather favourable, the height of the peak exceeding the value in the center of the trap by a factor

of 5.4 and the height of the smaller peak at the left mirror still by a factor of about 3. Thus, the idea of concentrating the neutron output by means of a hump in the magnetic field in front of one of the mirrors has been confirmed. Finally, the observed convergence of the iterations modelling the selfinteraction of the plasma (at least at sufficiently low angles of injection!) strengthens confidence in the stability of the version with simultaneous injection of deuterons and tritons.

We gratefully acknowledge numerous useful discussions with A. Ivanov and Yu. Tsidulko from the Budker Institute Novosibirsk during their stays at the FZR, sponsored by the Federal Ministry for Science and Education of the FRG.

References

[1] Int. Conf. Open Plasma Confinement Systems for Fusion, Novosibirsk 14-18 June 1993, Ed. A. A. Kabantsev, World Scientific 1994

[2] B. Weyssow and R. Balescu, J. Plasma Physics 35(1986)pp.449-471

[3] B. A. Trubnikov in Problems of Plasma Theory, ed. M. A. Leontovich, Vol. 1, Moscow, 1963, p.98 (russ.)

[4] B. N. Kozlov, Atomnaya energiya 12(1962)238 (russ.)

[5] R. K. Janev and J. J. Smith, Atomic and Plasma - Material Interaction Data for Fusion, Vol.4(Supplement to Nuclear Fusion), IAEA 1993

[6] V. G. Krasnoperov, V. N. Odinzov, V. N. Skripunov and V. V. Filatov, Engineering Problems in Designing a Neutron Source Based on a Gas Dynamic Trap Concept, Plasma Devices and Operations Vol. 3, No 2, 1993

[7] V. V. Mirnov, B. P. Nagorny and D. D. Ryutov, Preprint Budker Inst. Nucl. Phys. Nr. 84-40, Novosibirsk 1984

[8] Yu. Tsidulko, private communication

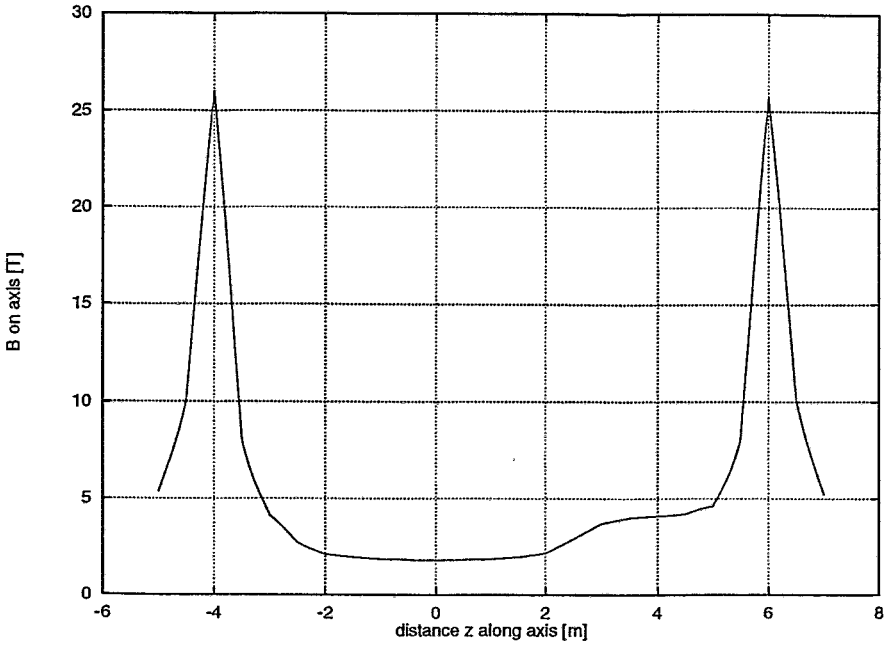

Figure 2: Dependence of the magnetic field on axis in Tesla on the distance z.

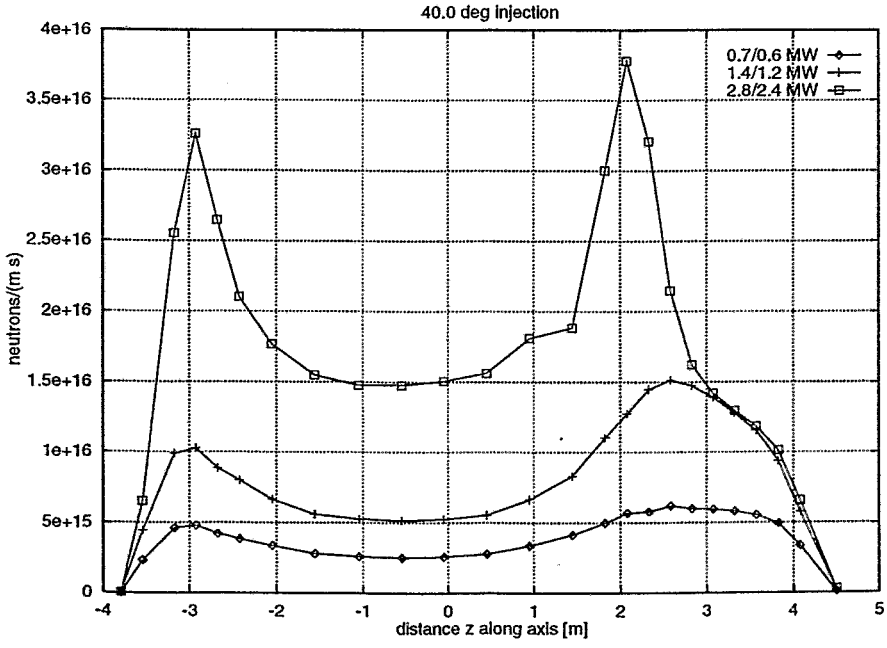

Figure 3: Distribution of the neutron source strength $[ns^{-1}m^{-1}]$ along the axis of the trap. The angle of injection for d as well as t neutrals is 40.0^0. The three graphs from lower to upper correspond to 5, 10 and 20% of the final input power.

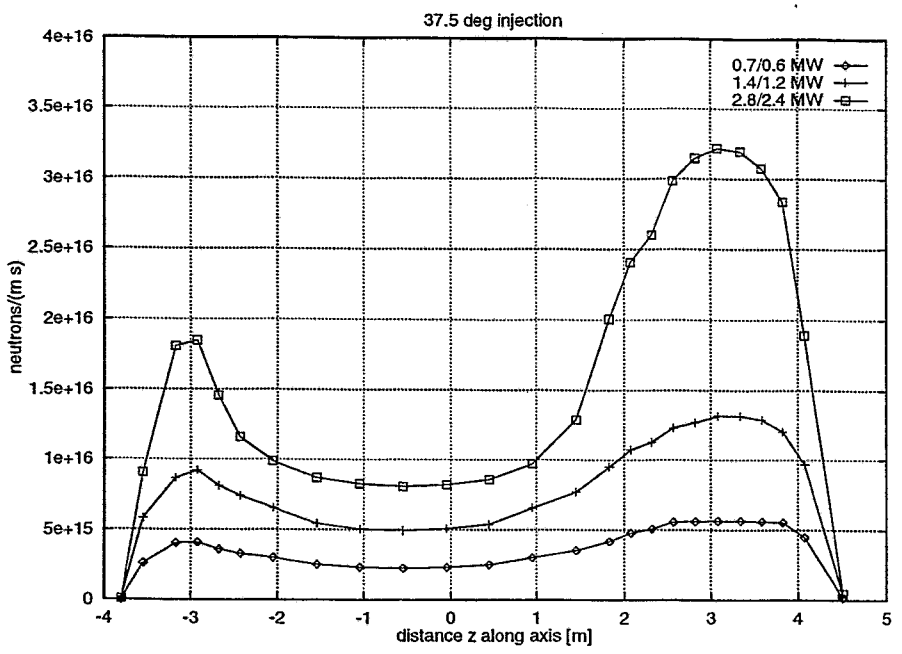

Figure 4: Distribution of the neutron source strength $[ns^{-1}m^{-1}]$ along the axis of the trap. The angle of injection for d as well as t neutrals is 37.5^0. The three graphs correspond to 5, 10 and 20% of the final input power.

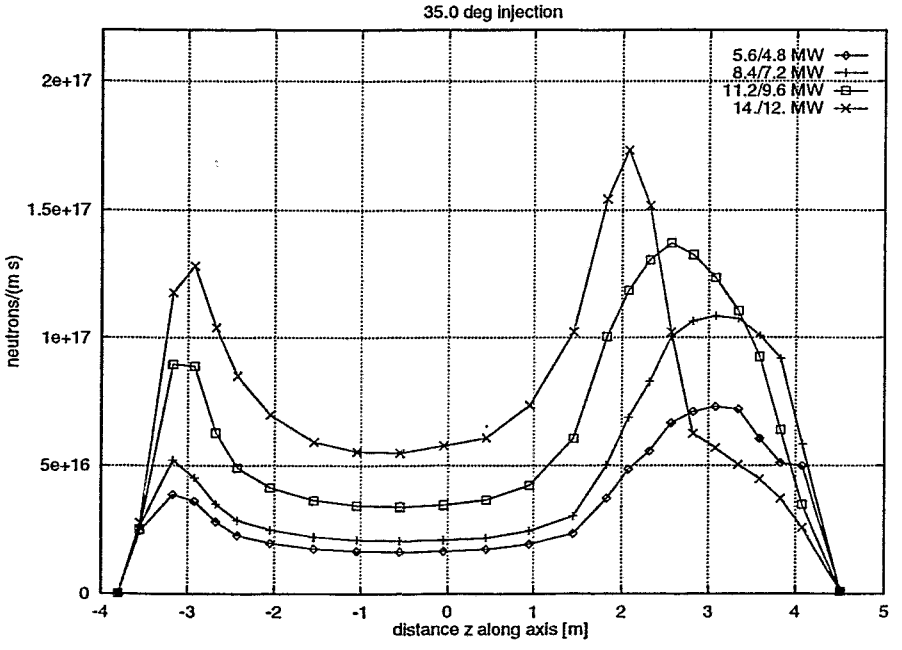

Figure 5: Distribution of the neutron source strength $[ns^{-1}m^{-1}]$ along the axis of the trap. The angle of injection for d as well as t neutrals is 35.0^0. The four graphs correspond to 40, 60, 80 and 100% of final input power.

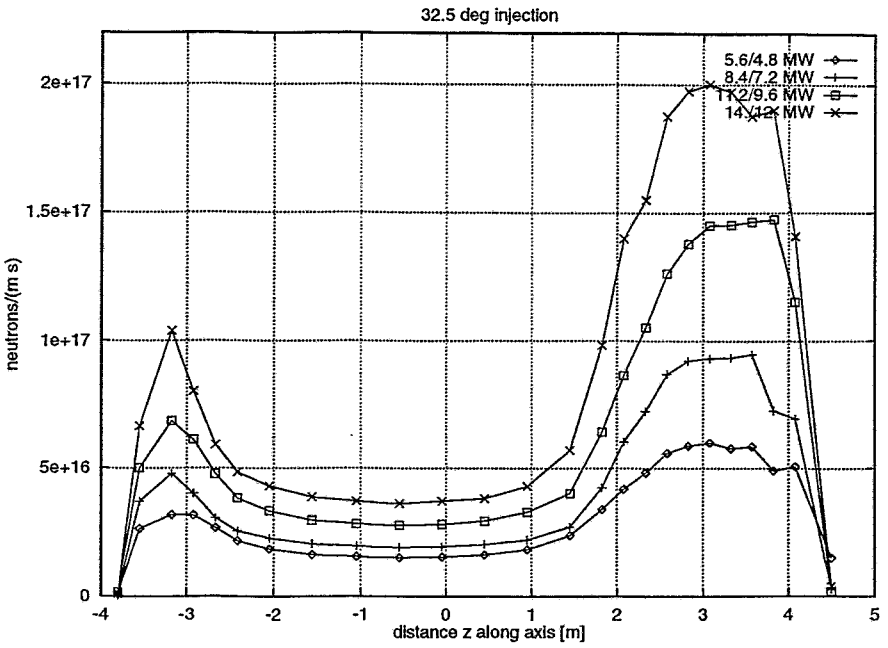

Figure 6: As previous figure, but injection angle reduced to 32.5^0.

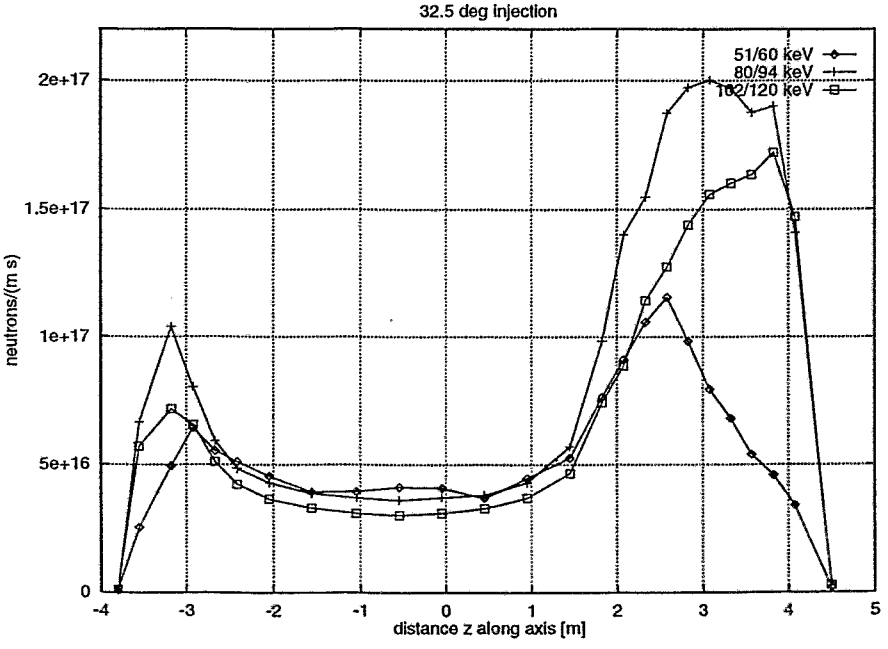

Figure 7: Neutron source strength distribution as in previous figures. The angle of injection is kept constant (32.5^0) as well as the input power (14.0/12.0 MW for deuterons/tritons respectively). The three graphs correspond to different injection energies (51.0/60.0, 80.0/94.0, 102.0/120.0 keV for deuterons/tritons respectively).

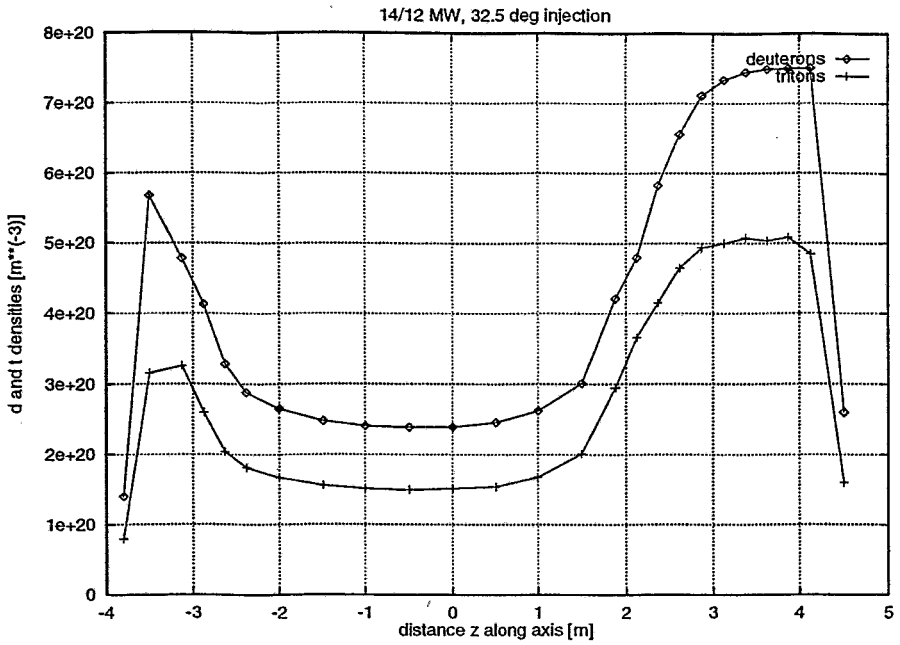

Figure 8: Distribution of the densities for deuterons and tritons for the case shown in fig.6 , upper curve (14/12 MW injection power for d/t, 32.5^0 injection angle).

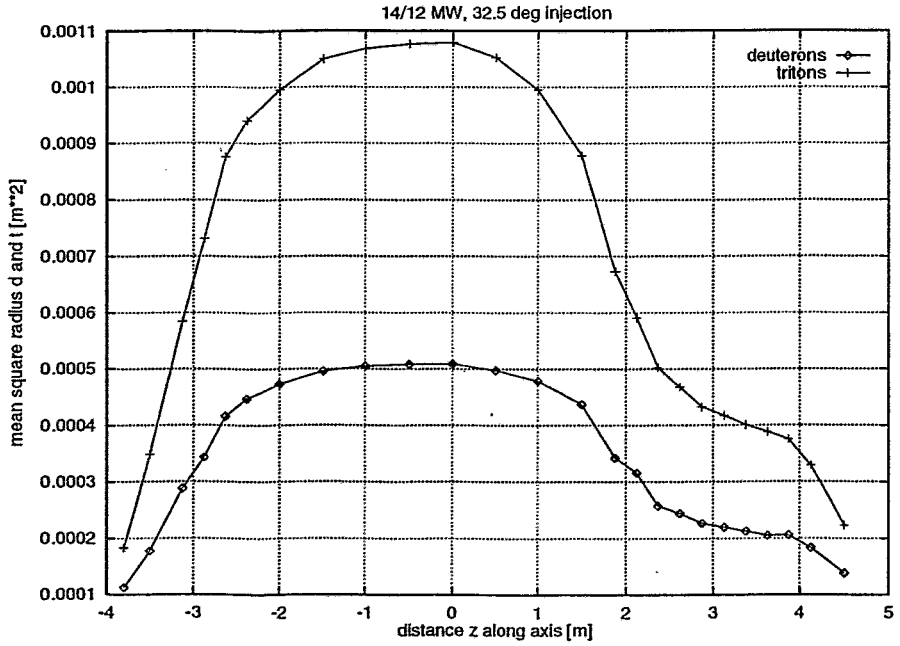

Figure 9: Distribution of mean square radius for deuterons and tritons. Same conditions as preceding fig.7

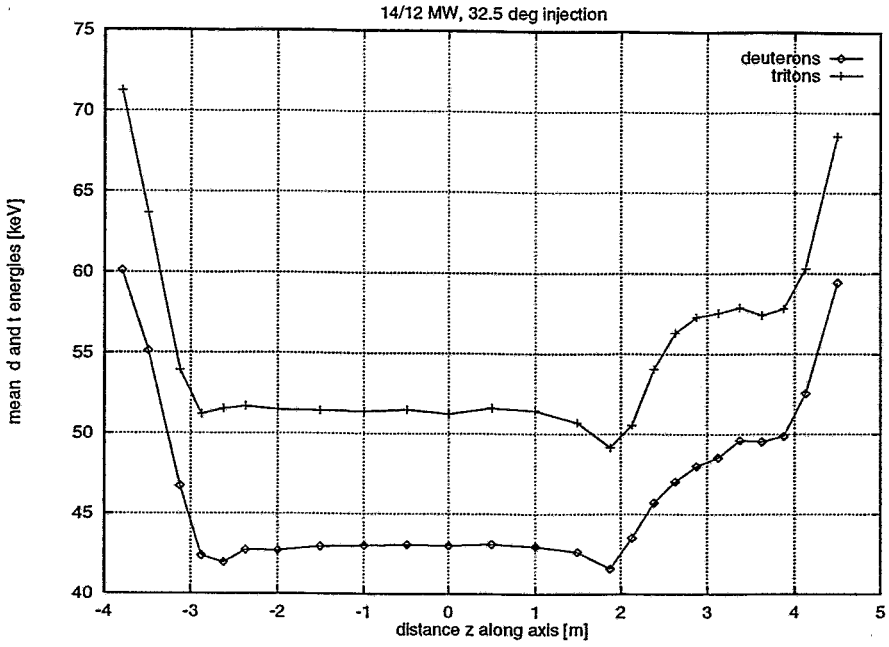

Figure 10: Distribution of mean energies for deuterons and tritons in the above case.

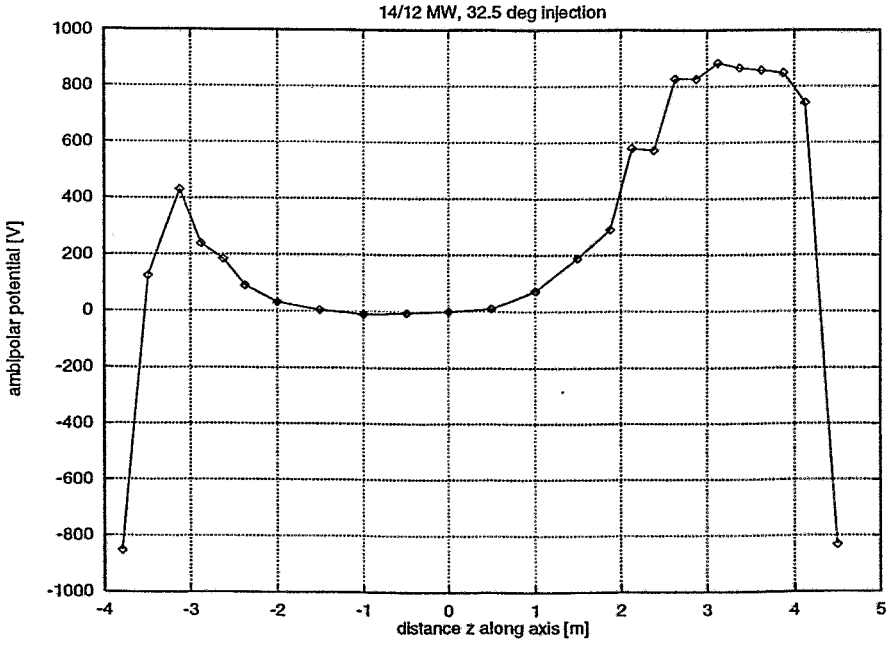

Figure 11: Distribution of ambipolar electric potential on the axis in the above case.

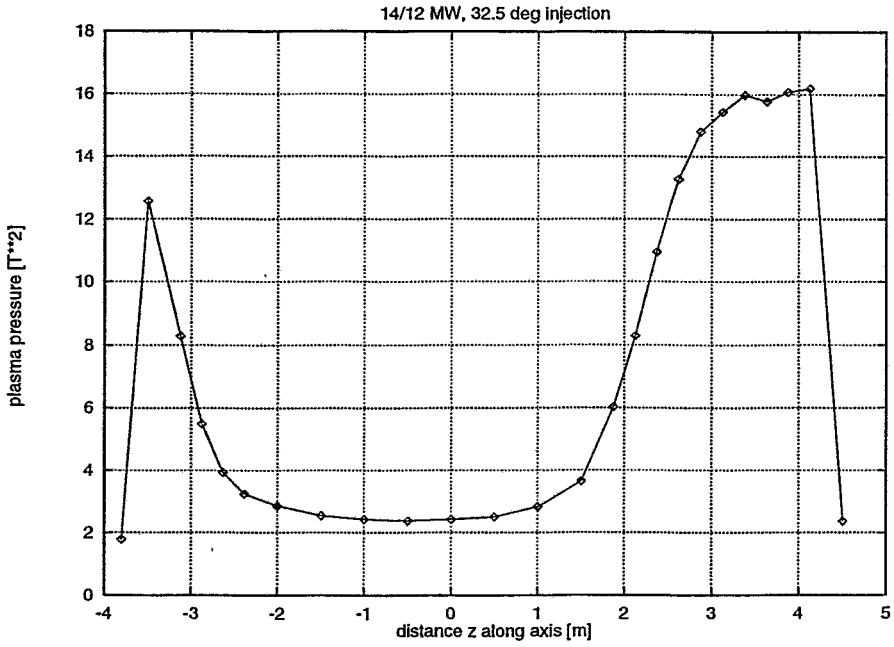

Figure 12: Distribution of total plasma pressure on the axis.

Index of notations

A auxiliary quantity, defined equ(25)
$\vec{B}$ magnetic field vector
B intensity of magnetic field $\vec{B}$
B_{ext} intensity of external magnetic field, created by coils
B_0 intensity B at origin $\rho = z = 0$
B_{th} intensity B at the threshold shown in fig.2 at $z = 4m, r = 0$
$\vec{b}$ direction unit vector of magnetic field
b_z, b_ρ components of $\vec{b}$ in cylinder coordinates
B_+, B_- derived magnetic field quantities defined equ(13)
c speed of light
e charge of particle
$\mathcal{E}$ total energy of particle
E_- derived electric field quantity defined equ(13)
E_r energy of relative motion in the binary reaction concerned
$f_\vartheta, f_\xi, f_\Delta$ normalized distribution functions of the indicated quantity
i particle index, $(i = d, t)$
m mass of particle
m_{dt} reduced mass of $d + t$ system, defined equ(44)
M generalized magnetic momentum of particle defined in equ(4) and equ(11)
$n_{el}, n_{ion}, n_d, n_t$ particle densuties of electrons, thermal ions, fast deuterons and fast tritons respectively
p_i, p_d, p_t pressure of particle i, d, t, $(i = d, t)$
P_d, P_t power of neutral d resp. t beam trapped in the plasma
$\vec{q}$ space vector of particle
T_e, T_i Temperatures of electrons and thermal ion component
U auxiliary quantity defined equ(20)
$\vec{v}$ velocity vector of particle
$\vec{v}_0$ velocity vector of impinging atom d or t
v_0 absolute value of above $\vec{v}_0$
$v_\perp$ value of velocity component perpendicular to field line $0 \leq v_\perp \leq \infty$
$v_\parallel$ velocity component parallel to field line, $-\infty \leq v_\parallel \leq \infty$
$\vec{Y}$ vector of guiding centre space coordinates
Y_ρ, Y_ψ, Y_z components of the above vector in cylinder coordinates
z see ρ
γ azimuthal angle of deflection, $0 \leq \gamma \leq 2\pi$
ϵ small parameter introduced equ. (2), after expansion to first order in ϵ to be set $\epsilon = 1$
$\delta(x)$ Dirac deltafunction
Δ relative variation of M, defined equ(23)
ζ_d, ζ_t cosine of pitch angle for d and t, defined equ(41)
$\bar{\Delta}$ mean of above quantity Δ, defined equ(29)
ϑ polar angle of deflection, $0 \leq \vartheta \leq \infty$ formally
$\langle\vartheta^2\rangle$ mean square angle of deflection $\ll 1$
θ angle of injection of neutral beams
μ magnetic momentum of particle def. equ.(1)
$\xi = \cos\gamma$, equ(24)
ρ, ψ, z cylinder coordinates of particle space vector $\vec{q}$
σ^2 mean square od Δ, defined equ(30)
$\sigma_{cx}, \sigma_{ion}$ cross-sections for charge exchange and ionization of the impinging neutral D or T atom in the plasma
σ_{dt} reaction cross-section of the D(t,n)-reaction, see equ(45)
Σ_0 macroscopic total ionization cross-section for the impinging D or T atom
τ_b relaxation time for energy loss
τ_d relaxation time for deflection
φ phase angle of particle (angle between component of the velocity perpendicular to the magnetic field and the binormal of the fieldline)
Φ guiding centre phase, defined equ(5) and equ(12)
ϕ electric potential
ψ see ρ
Ω particle Larmor frequency defined in equ(2)